

MEASUREMENT AND MODELING OF DENSITY-SENSITIVE LINES OF Fe XIII IN THE EXTREME ULTRAVIOLET

N. YAMAMOTO¹

Nagoya University, Nagoya, Japan

T. KATO, H. FUNABA, K. SATO, N. TAMURA, AND S. SUDO

National Institute for Fusion Science, Oroshi-cho, Toki, Gifu, 509–5292, Japan

AND

P. BEIERSDORFER² AND J. K. LEPSON

Space Sciences Laboratory, University of California, Berkeley, CA 96720

Received 2008 January 31; accepted 2008 July 8

ABSTRACT

We present an analysis of the spectral emission of Fe XIII near 200 Å. High-resolution spectra were recorded at two densities ($\sim 2 \times 10^{11}$ and $\sim 10^{13}$ cm⁻³) in the laboratory and compared to collisional radiative model calculations based on the CHIANTI database, and to models using atomic data from distorted-wave and *R*-matrix calculations. The Fe XIII lines in this wavelength range are sensitive indicators of plasma density below $\sim 10^{11}$ cm⁻³. The laboratory data thus test calculations in the astrophysical high-density limit. Significant differences between the measurements and models were found for several line ratios. Differences in the wavelengths employed in the different models also changed the agreement with the measurements. The best agreement was found for comparisons with CHIANTI.

Subject headings: atomic data — atomic processes — line: formation — line: identification — plasmas — ultraviolet: general

Online material: color figures

1. INTRODUCTION

The spectrum of Fe XIII near 200 Å provides important markers for the density of solar and stellar coronal plasma. These lines have been observed, for example, by the *Solar EUV Rocket Telescope and Spectrograph (SERTS)* in the Sun, and by the *Extreme Ultraviolet Explorer (EUVE)* in Procyon and ϵ Eridani (Thomas & Neupert 1994; Young et al. 1994; Schmitt et al. 1996), and have been used to derive electron densities in the range $8.8 < \log n_e < 9.8$. This spectral region is also being observed with the *Hinode* satellite, which was launched in 2006 to study the Sun (Watanabe et al. 2007). One of the two channels of the EUV Imaging Spectrometer (EIS) aboard *Hinode* is sensitive to the wavelength range from 170 to 210 Å. Thus, the Fe XIII emission plays an important role in the observations carried out with *Hinode*.

Recent analyses have revealed discrepancies among the available atomic data for Fe XIII that may lead to difficulties in interpreting observed spectra (Landi 2002; Young 2004; Keenan 2007). In fact, such difficulties had been noted earlier, for example by Brickhouse et al. (1995), Landi & Landini (1997), and Young et al. (1998). The recent comparison by Landi (2002) of modeling calculations with SERTS observations has not only identified problems with the atomic data, but has also led to a set of recommended Fe XIII lines thought to be free of atomic physics problems and useful as diagnostics of the electron density.

Laboratory data have been particularly useful for identifying specific problems with atomic models and for calibrating density and temperature diagnostics (Beiersdorfer 2003). Because plasma parameters are known from diagnostics that do not rely on atomic data, the reliability of spectral models can be assessed beyond

performing a consistency check. In this paper, we present laboratory measurements of the Fe XIII emission generated by the Large Helical Device (LHD) at the National Institute for Fusion Science (NIFS) in Toki and the EBIT-II electron beam ion trap at the Lawrence Livermore National Laboratory (LLNL). We compare these measurements to new calculations based the Hebrew University-Lawrence Livermore Atomic Code (HULLAC; Bar-Shalom et al. 2001), which uses the distorted-wave approximation to compute excitation cross sections; and calculations by Aggarwal & Keenan (2004), based on atomic data generated by the Dirac Atomic *R*-matrix Code (DARC). We also compare our measurements to results from the CHIANTI spectral modeling code (Landi et al. 2006).

2. MEASUREMENTS

2.1. Electron Beam Ion Trap Data

The first set of spectral data were recorded at the EBIT-II electron beam ion trap at the University of California Lawrence Livermore National Laboratory. This machine has been used for a variety of laboratory astrophysics measurements in the past (Beiersdorfer 2003; Lepson et al. 2008), and operates at densities below 10^{12} cm⁻³ (Chen et al. 2004).

The present measurements utilize techniques similar to those described in earlier measurements of the iron emission (Drake et al. 1999; Beiersdorfer et al. 1999b; Lepson et al. 2002). Iron was injected into the trap in form of iron pentacarbonyl via a gas injector. The electron beam energy ranged from 363 to 513 eV, i.e., above the ionization energy of 323 eV needed to produce Fe¹²⁺ ions. The higher energy is sufficient to produce charge states as high as Fe¹⁶⁺. Spectral blending with charge states higher than Fe¹²⁺ is, however, not a problem in the region of interest. By contrast, the emission from lower charge states is readily observed,

¹ Current address: ILE, Osaka University, Osaka, Japan.

² Also at: Lawrence Livermore National Laboratory, Livermore, CA 94550.

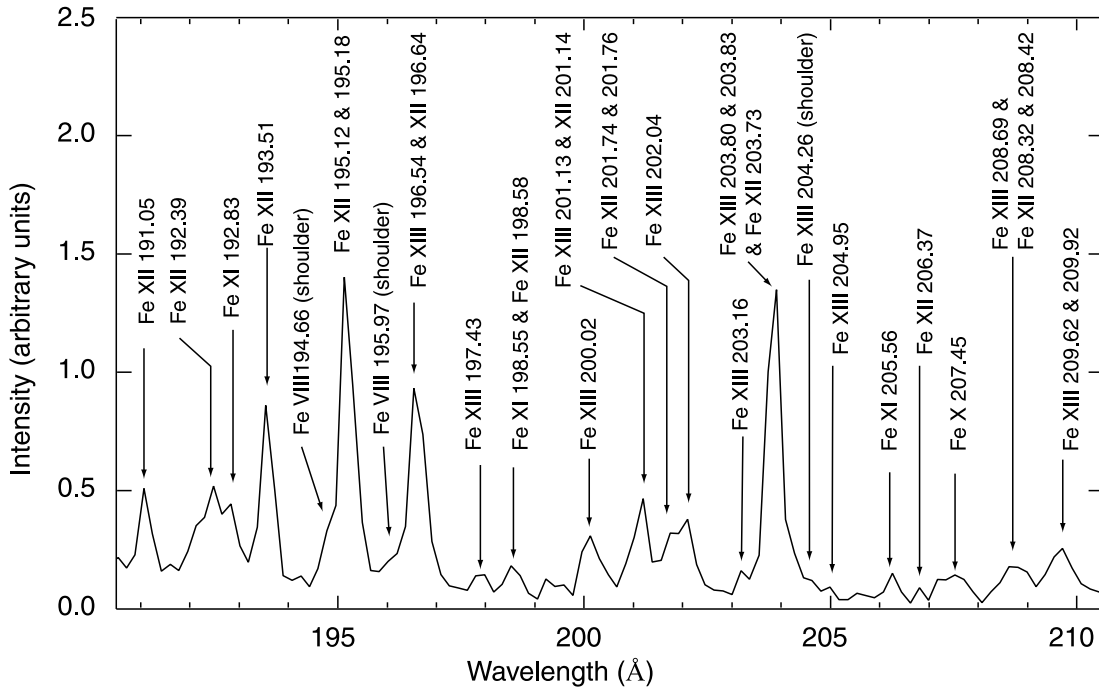


FIG. 1.—Iron spectrum from 190.5 to 210.5 Å measured at the EBIT-II electron beam ion trap facility, and line identifications. Wavelengths given are from the CHIANTI database.

because of the fact that neutral iron is continuously injected into the trap. Moreover, the trap is periodically emptied and filled (once every few seconds), and the measurements are time-integrated over the ionization phase.

The spectra were recorded with the grazing-incidence spectrometer described by Beiersdorfer et al. (1999a). The instrument employs an average 1200 line mm^{-1} flat-field grating developed by Harada & Kita (1980), with a 3° angle of incidence. Readouts were taken with a back-illuminated, liquid-nitrogen-cooled CCD camera with a 1 inch (2.54 cm) square array of 1024×1024 pixels. The instrumental resolving power ($\lambda/\Delta\lambda$, where $\Delta\lambda$ is the full width at half-maximum) is ~ 600 at 200 Å.

A foil composed of a 2000 Å thick aluminum layer on top of 1000 Å of paralene was placed in front of the grating in order to screen out emission from lines with wavelength below 170 Å. This was necessary to avoid spectral contamination from higher energy iron lines that would show up in second, third, or fourth order reflection. Although emission among levels of principal quantum number $n = 3$ of interest here is typically much stronger than emission from the $n = 4$ (or higher) level to the $n = 3$ level, blending with higher order lines can otherwise be significant nonetheless, especially when studying weak 3–3 lines.

The wavelength scale was established using the well-known K-shell emission lines of nitrogen, in particular the N VII Ly α line and the N VI resonance line commonly referred to as w , as described by Beiersdorfer et al. (1999a), observed in higher (7th, 8th, and 9th) orders. The energies of these lines are high enough to pass through the aluminum filter without appreciable attenuation. The wavelengths of the iron emission lines in this wavelength region are well known, and we have not attempted to improve on those data.

Spectra were also taken without an active trap, i.e., without a potential applied to the trap electrodes. These spectra enabled us to determine the level of background emission (including visible light from the electron-gun filament, to which the CCD camera is

sensitive), which was then subtracted from the iron spectra to yield background-corrected spectra.

Figure 1 shows the iron spectrum taken on EBIT-II in the range from 190 to 210 Å. The spectrum represents the sum of about 20 spectra after background subtraction. The spectral emission is dominated by Fe XII and Fe XIII, as shown by the two strongest peaks at 195.1 and 203.8 Å. Essentially all lines in the spectrum have been identified, as illustrated in Figure 1, where each peak is identified with known iron lines. The spectrum includes lines from all charge states between Fe VIII and Fe XIII.

For identification we relied on the atomic data provided by the CHIANTI spectral model. To do so, we used the predicted emission at the high-density limit (that is, high-density compared to typical coronal plasmas) of 10^{15} cm^{-3} . Using these data at this limit is justified, as little density dependence can be found above 10^{11} cm^{-3} , i.e., for the density of the present measurements on EBIT-II estimated at $2 \times 10^{11} \text{ cm}^{-3}$. In fact, the CHIANTI intensities at the high-density limit reproduce the measured intensities very well, as shown in § 4.

2.2. Large Helical Device Stellerator Data

The second set of spectral data were recorded at the LHD at NIFS (Motojima et al. 2005). The magnetic field used for plasma confinement in this machine is generated with a superconducting electromagnet, which makes steady state operation possible. The helical coils produce a magnetic field up to 3 T. Here we report on the spectrum observed in shot #66810, where an iron pellet was injected into LHD. The discharge in this shot lasted about 4.5 s and attained a line-averaged density of about $2.5 \times 10^{13} \text{ cm}^{-3}$. The temperature reached 2–3 keV during the main part of the discharge; this temperature is, however, greatly reduced during the plasma decay phase after the end of the heating by neutral beam injection. The line-averaged electron density also drops after neutral beam heating, and may be as low as 10^{13} cm^{-3} .

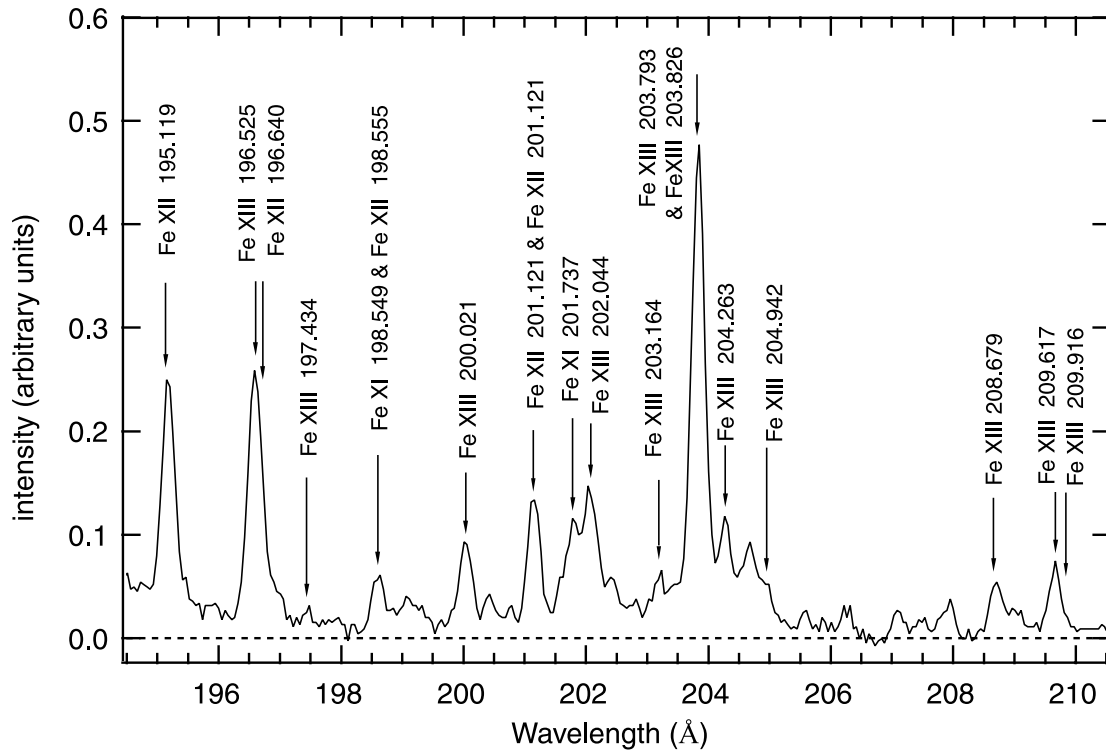


Fig. 2.—Iron spectrum from 194.5 to 210.5 Å measured at LHD. Wavelengths given are from the NIST database.

By recording spectra throughout the discharge every 0.1 s, spectra with different ionization balances are obtained. For example, the emission from Fe xxiv dominates the spectral region near 200 Å during the main part of the discharge. In fact, essentially no other lines of iron are seen during these times. After the end of the plasma heating, the temperature is sufficiently low to see emission from Fe viii through Fe xiii, similar to the measurements made on EBIT-II.

The present measurements were made with the SOXMOS EUV grazing-incidence spectrometer (Schwob et al. 1987), covering the wavelength range from 158 to 214 Å. The instrument utilized a 600 lines mm⁻¹ grating. It was operated with a 10 μm slit, which provided a resolving power of ~780 throughout the wavelength range of interest. This resolution is somewhat higher than that of the EBIT-II measurements. Additional measurements were made using a 133 lines mm⁻¹ grating. Although these measurements had considerably lower resolving power, they confirmed line identification and ionization balance evolution during the discharge.

No filters were used to screen out lines from second order. Second-order lines were only identified in spectra from hot plasmas, and were found to emanate from such ions as Fe xviii at 187.8 Å and Fe xix at 216.7 Å.

Because iron is not, or is only weakly, seen in LHD plasmas, the iron concentration was increased by pellet injection. For this purpose, plastic pellets with an iron core called TESPEL were used (Tamura et al. 2003). Iron thus dominates the emission in the region of interest, and essentially no lines from other elements are seen, with the possible exception of C v lines near 227 Å and above.

The wavelength scale was determined using the strong Fe lines, as the wavelengths of the iron emission lines in this spectral region are well known. We used 15 Fe ion emission lines to make a calibration curve. The main lines used to determine the wavelength scale are Fe ix (171.073 Å), Fe xii (195.119 Å), Fe xiii (203.800 Å), and Fe xiv (211.331 Å).

Figure 2 shows the iron spectrum in the range from 190 to 210 Å measured on LHD. The spectrum represents the sum of the data recorded between 4.3 and 4.4 s. The spectral emission is dominated by Fe xiii, which produces the strongest feature in the spectrum at 203.8 Å. Lines from Fe xii are also visible, and lines from other charge states as low as Fe viii can be identified. As was the case with the EBIT-II data, essentially all lines in the spectrum have been identified, as indicated in Figure 2.

3. MODEL SPECTRA

We applied three radiation models to analyze the measured spectra from EBIT-II and LHD. Two of the three models are our own models using different atomic data sets, i.e., from Aggarwal & Keenan (2004) and from HULLAC (Bar-Shalom et al. 2001). The third model is CHIANTI (Dere et al. 1997; Landi et al. 2006).

We constructed an original collisional-radiative model of Fe ions including the fine-structure levels up to $n = 5$. This model includes processes of excitation and de-excitation by electron impact, radiative decay, radiative recombination, ionization, three-body recombination, and autoionization, as well as dielectronic capture and dielectronic recombination. Transition probabilities and cross sections of these processes were calculated with the HULLAC code (Bar-Shalom et al. 2001). The data obtained with an *R*-matrix code by Aggarwal & Keenan (2004) were used to calculate the electron impact excitation rate coefficients and radiative transition probabilities for the transitions between the $3s^23p^2$, $3s3p^3$, and $3s^23p3d$ states. The rate coefficients were evaluated by Skobelev et al. (2007) and fitted by analytical functions. The excitation rate coefficients for proton impact evaluated by Skobelev et al. (2006) are also included for the transitions between fine-structure levels of the ground-state configuration. The population densities needed to calculate line intensities are obtained by solving the coupled rate equations for each energy level. The calculation of the population density includes both an

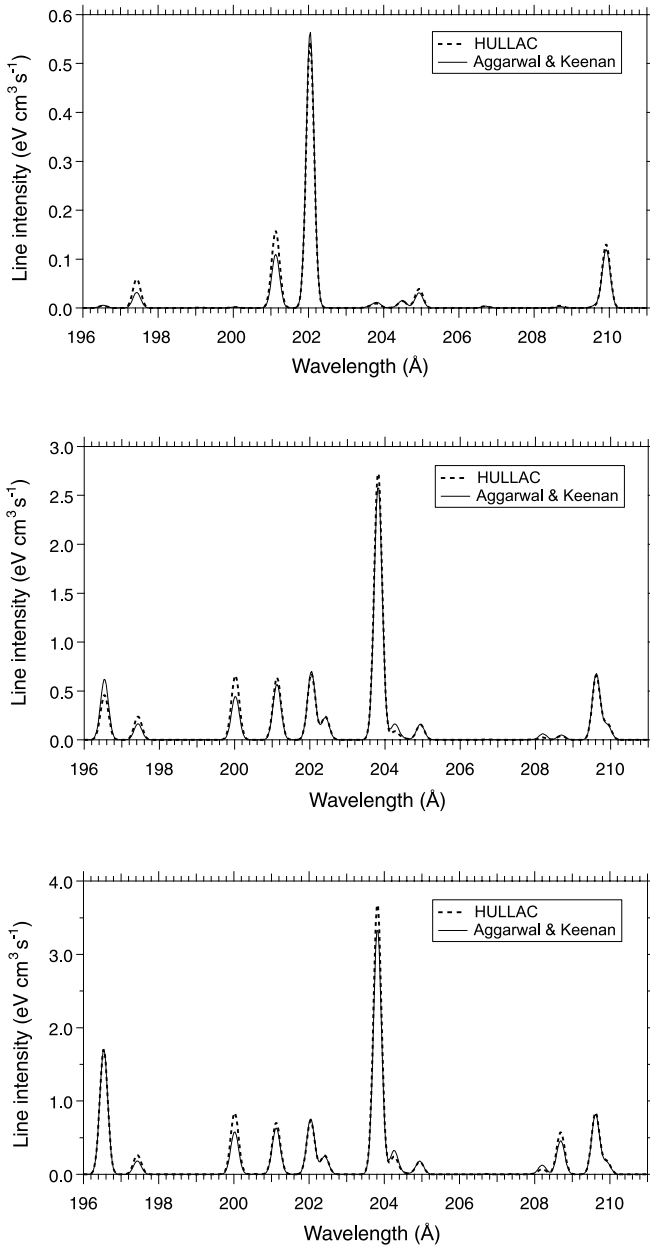


FIG. 3.—Line emission of Fe XIII at $N_e = 10^6 \text{ cm}^{-3}$ (top), $N_e = 10^{10} \text{ cm}^{-3}$ (middle), and $N_e = 10^{15} \text{ cm}^{-3}$ (bottom) in the range of 196–211 Å using atomic data by Aggarwal & Keenan (solid red line) and HULLAC (dashed black line).

ionization and a recombination component in our model. In this paper the population densities during the ionizing phase are applied to the analysis of the measured spectra.

The calculated spectra of Fe XIII at $N_e = 10^6$, 10^{10} , and 10^{15} cm^{-3} in the wavelength range of 196 to 211 Å are shown in Figure 3. At low-density conditions, the lines excited from the lowest lying ground state ($3s^23p^2 \ ^3P_0$) are strong, e.g., the line at 202.044 Å ($3s^23p^2 \ ^3P_0 - 3s^23p3d \ ^3P_1$). With increasing electron density, the population densities of ground-state fine-structure levels other than $J = 0$ (i.e., $3s^23p^2 \ ^3P_1$, 3P_2 , 1D_2 , 1S_0) increase due to the excitation from the $J = 0$ ground state. Therefore, the intensities of many other lines increase, since their upper states are excited from these higher-lying fine structure levels at the higher electron densities.

Figure 3 shows spectra of Fe XIII using the two atomic data sets: (1) calculated by the HULLAC code, and (2) calculated by Aggarwal & Keenan for collisional excitation between $3s^23p^2$,

$3s3p^3$, and $3s^23p3d$ levels and by HULLAC for the other transitions. Most of the Fe XIII lines in the range of 195–210 Å by the HULLAC code are stronger by $\sim 10\%$ than those in Aggarwal & Keenan, except for the 196.5 and 202.0 Å lines. We note that the intensities of other lines are in good agreement within 10%. The intensity ratios of all lines in the range of 194–212 Å have essentially no temperature dependence. The dependence of the intensity ratios on the electron density agrees well for the two models, except for one particular transition between two singlet states. In particular, the density dependence of the intensity of the singlet line at 196.5 Å ($^1D_2 - ^1F_3$) predicted by the two models does not agree well at the low densities, HULLAC being about 50% larger (not visible at the scale used in Fig. 3a), but agreement is achieved in the high-density limit. The intensity of the 200.0 Å line of Aggarwal & Keenan is 30% larger than that of HULLAC, due to the difference of radiative transition rate between two calculations.

In our models we use the NIST database for setting the wavelength of each line. The NIST wavelengths are mostly in good agreement with those given in CHIANTI. The main exception in Fe XIII is the $3s^23p^2 \ ^3P_1 - 3s^23p3d \ ^3P_0$ transition. For this transition, CHIANTI uses a wavelength of 203.164 Å, while it is listed as 202.424 Å in the NIST database. For Fe XII we find three exceptions. These are the $3s^23p^3 \ ^2P_{1/2} - 3s^23p^23d \ ^2P_{1/2}$, $3s^23p^3 \ ^2P_{3/2} - 3s^23p^23d \ ^2S_{1/2}$, and $3s^23p^3 \ ^2D_{5/2} - 3s^23p^23d \ ^2D_{5/2}$ transitions. CHIANTI lists their wavelengths as 201.740, 201.760, and 203.728 Å, respectively; the NIST database, based on the compilation by Shirai et al. (2000), lists their wavelengths as 202.090, 200.346, and 203.272 Å, respectively.

4. COMPARISON OF THE MEASURED SPECTRA WITH THE MODELING RESULTS

Table 1 lists the line intensities of the strong lines in the measured Fe XIII spectra from EBIT-II and LHD. The intensities are normalized to the intensity of the line at 202.04 Å ($^3P_0 - ^3P_1$), which was chosen because this line has essentially no density dependence. Line intensities of EBIT-II and LHD agree within 10%–20%. The intensity of the 204.26 Å line ($^3P_1 - ^1D_2$) measured on LHD is stronger by 45% than that measured on EBIT-II. On the other hand, the intensities of the 196.54 Å line ($^1D_2 - ^1F_3$), the 203.80 Å line ($^3P_2 - ^3D_3$), and the 209.62 Å line ($^3P_1 - ^3P_2$) measured on EBIT-II are stronger than those measured on LHD. These differences, however, are generally within the error bars.

Table 1 also gives the intensities calculated by our own two models and CHIANTI. Because the Fe XIII lines are blended with those of Fe XII, and since the wavelengths of Fe XII differ between CHIANTI and NIST, the line intensity ratios are sensitive to which sets of wavelengths are used. We therefore used the CHIANTI wavelengths to derive the measured line intensity ratios in Table 1. A comparison with the measured intensities from both EBIT-II and LHD shows that the predicted intensities from CHIANTI match the measurements well. Only the intensity predicted for the line at 208.69 Å is somewhat too high. The models based on collision strengths from HULLAC and Aggarwal & Keenan predict an intensity that is even higher than that from CHIANTI, and thus differ even more from the measurements. These two models also significantly overpredict the intensity of the Fe XIII lines at 197.43, 200.02, and 209.62 Å. Moreover, they underpredict the intensity of the Fe XIII line at 208.69 Å. This means they differ from the measured values for almost half of the lines.

A graphical comparison between the measurements and the modeled spectra is shown in Figures 4 and 5. Since the results based on HULLAC and Aggarwal & Keenan are not very different, as already shown in Figure 3, we only compare to the spectral fit with atomic data by Aggarwal & Keenan in Figures 4

TABLE 1
COMPARISON OF MEASURED LINE INTENSITIES WITH THREE DIFFERENT MODELS

Wavelength ^a (Å)	EBIT-II	LHD	HULLAC	Aggarwal & Keenan	CHIANTI
196.54.....	2.70 (0.15) ^b	1.98 (0.16) ^b	2.40	2.33	1.99
197.43.....	0.06 (0.05) ^c	0.09 (0.05)	0.37	0.33	0.14
200.02.....	0.75 (0.17)	0.57 (0.20)	1.16	0.98	0.69
201.13.....	0.74 (0.22) ^{d,g}	0.56 (0.20) ^{d,g}	0.97	0.85	0.69
202.04.....	1.00 (0.19)	1.00 (0.17)	1.00	1.00	1.00
203.16.....	0.24 (0.22)	0.36 (0.20)	0.36	0.34	0.28
203.80+203.83.....	3.95 (0.21) ^e	3.36 (0.20) ^e	4.96	4.44	3.70
204.26.....	0.44 (0.18)	0.81 (0.20)	0.33	0.29	0.66
204.95.....	0.17 (0.06)	0.30 (0.18)	0.24	0.21	0.21
208.69.....	0.39 (0.07)	0.36 (0.19)	0.76	0.68	0.58
209.62.....	0.83 (0.19) ^f	0.52 (0.20)	1.11	0.98	0.65

The intensities are normalized to the line Fe XIII $\lambda 202.04$ (${}^3P_0-{}^3P_1$). The uncertainties in the measured intensities are given in parentheses.

^a CHIANTI (v. 5.2; Dere et al. 1997; Landi et al. 2006).

^b Contribution from Fe XII removed.

^c Contribution from Fe VIII removed.

^d Contribution from Fe XII removed.

^e Contribution from Fe XII removed.

^f Contribution from $\lambda 209.92$ removed.

^g Contribution from $\lambda 201.12$ included.

and 5. The biggest difference is found for the line at 204.26 Å ($3s^23p^2\ {}^3P_1-3s^23p3d\ {}^1D_2$), near the strongest line at 203.8 Å. The intensity of the 204.26 Å line calculated from the Aggarwal & Keenan atomic data is more than a factor of 2 smaller than that from CHIANTI. The measured spectra from EBIT-II agree with

CHIANTI better than with the model based on the Aggarwal & Keenan data.

In addition to those differences, which arise because of the differences in the calculated intensities, and which were already noted in Table 1, there are also differences that stem from the

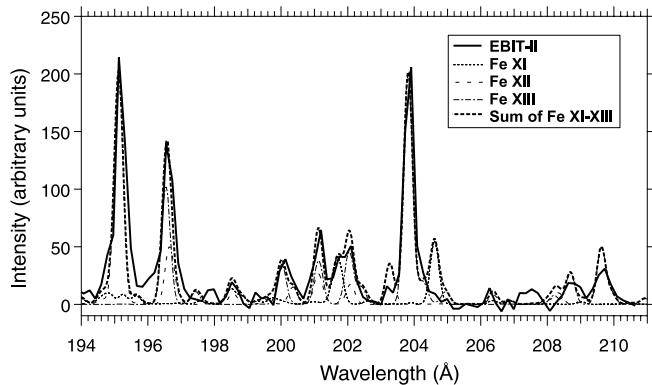
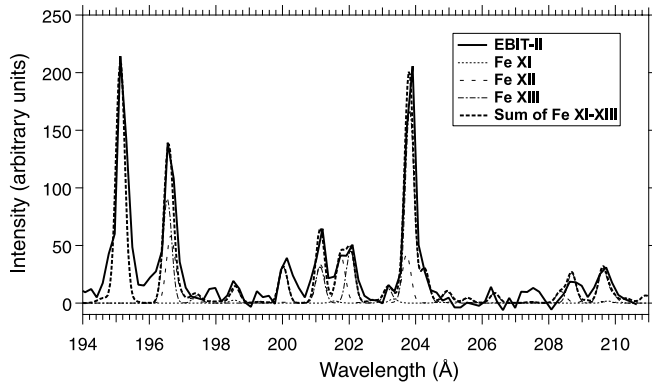


FIG. 4.— Comparison of EBIT-II measurements with spectral models. *Top*: EBIT-II spectrum fitted by the CHIANTI model for $T_e = 137$ eV and $N_e = 10^{15}$ cm⁻³. *Bottom*: EBIT-II spectrum fitted by our model using atomic data by Aggarwal & Keenan for $T_e = 137$ eV and $N_e = 10^{15}$ cm⁻³. [See the electronic edition of the Journal for a color version of this figure.]

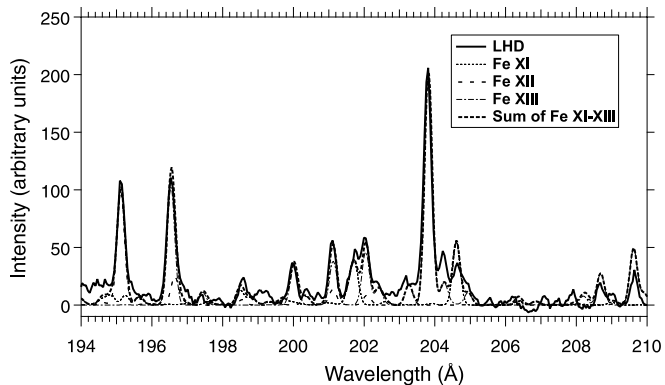
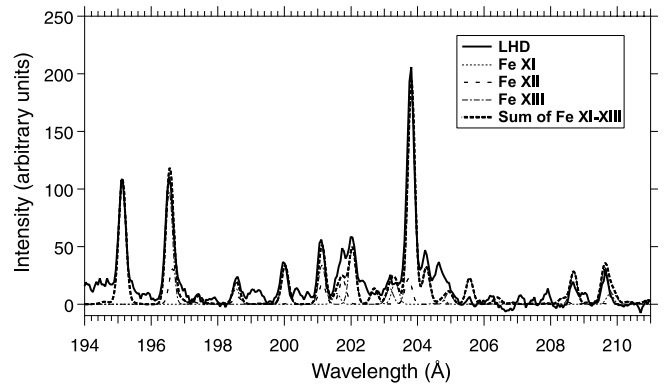


FIG. 5.— Comparison of LHD measurements with spectral models. *Top*: LHD spectrum fitted by the CHIANTI model for $T_e = 137$ eV and $N_e = 10^{15}$ cm⁻³. *Bottom*: LHD spectrum fitted by our model using atomic data by Aggarwal & Keenan for $T_e = 137$ eV and $N_e = 10^{13}$ cm⁻³. [See the electronic edition of the Journal for a color version of this figure.]

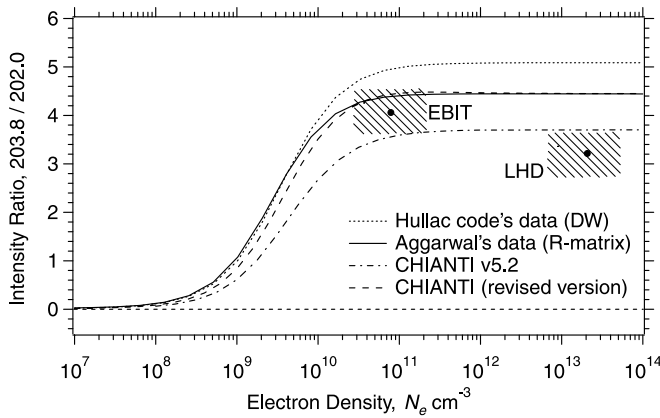


FIG. 6.— Electron density dependence of the intensity ratio $I_{203.8}/I_{202.0}$ of the Fe XIII lines at 203.8 and 202.0 Å. [See the electronic edition of the Journal for a color version of this figure.]

differences in the assumed line positions. In the case of Fe XIII, only one line takes on a different wavelength value between the CHIANTI model and our model, as discussed above. In the case of Fe XII, however, there are three lines that have different wavelengths. This change in line position produces a poor fit of the EBIT-II spectrum when using the NIST wavelengths and the collisional data of Aggarwal and Keenan, while the CHIANTI data produces a good fit. The reason for the poor fit is that the Fe XII line at 203.7 Å, where it blends with the strongest Fe XIII line, moves to 203.3 Å, where there is too little flux in the experimental spectrum to accommodate a strong line. At the same time, the two Fe XII lines at 201.75 Å, where they nicely fit the EBIT-II spectrum, split. One moves to 200.4 Å, where it indeed produces a much better fit to the data. The other moves on top of the neighboring Fe XIII line at 202.1 Å. The void these two Fe XII lines leave behind at 201.75 Å is filled in our model by an Fe XI line, which does not exist in CHIANTI. While this works well, our model predicts an even stronger Fe XI line at 204.6 Å, which is clearly much too strong to match the data. This is less of an issue in the case of the LHD spectrum, as there is sufficient flux at 204.6 Å to justify a large Fe XI line. Apart from the Fe XI contribution, the LHD spectrum can be fit essentially equally well by either CHIANTI or our model. In fact, here it appears that the CHIANTI intensities, augmented by our Fe XI calculations together with the NIST wavelengths for the Fe XII and Fe XIII lines, would produce the best fit. This discussion shows that it is imperative not only to produce accurate collisional data, but also to remove any uncertainty in the wavelengths of these lines.

The intensity ratio of the Fe XIII line at 203.8 Å to the Fe XIII line at 202.0 Å is used as a density diagnostic for the solar transition region. The calculated ratios based on the three models are shown in Figure 6 along with the measured ratios. As for Table 1, the measured line ratios were derived by adopting the CHIANTI wavelengths. The ratios using the HULLAC data and the Aggarwal & Keenan data agree well at densities below $5 \times 10^9 \text{ cm}^{-3}$. Their predictions disagree in the high-density limit by 10%. The density rise in the line ratio predicted by CHIANTI v5.2 appears at higher densities than that given by the HULLAC and Aggarwal & Keenan models. The result from CHIANTI v5.2 in the high-density limit is lower than that from the Aggarwal & Keenan model by about 15%. However, the ratio from new version of CHIANTI is in very good agreement with that from the Aggarwal & Keenan model. The experimental intensity ratio obtained from EBIT-II is slightly larger than the value from CHIANTI v5.2, and roughly overlaps with our model and a new version of CHIANTI within

the error bar, but does not overlap with our HULLAC model. The ratio from LHD is slightly smaller than the value from CHIANTI v5.2, and does not overlap with either of our models or a new version of CHIANTI. These discrepancies might be due to the blend of O V lines at around 202.0 and 203.8 Å from LHD plasma. The O V line intensities from LHD seem to vary by experimental shot. The observed intensity ratios of $\lambda 203.8/\lambda 202.0$ changed from 2.6 to 5.3 in different shots.

The density dependence of the $\lambda 203.8/\lambda 202.0$ ratio arises because of an increase in the population of the higher-lying fine-structure levels as the density increases. Proton excitation as well as electron excitation can contribute to collisional rearrangement between fine-structure levels, which may matter, in principle, in the Sun as well as in LHD plasma. However, the temperature range of interest is about 130–140 eV, where proton excitation is not strong. Proton excitation becomes comparable to electron excitation only for an electron temperature higher than 200 eV.

5. DISCUSSION AND SUMMARY

Our study of the Fe XIII line emission found agreement within error bars between our measurements from EBIT-II and the CHIANTI model (new version) and our model based on *R*-matrix calculation by Aggarwal & Keenan. Agreement appears to be less good for the models we generated using the atomic data from HULLAC.

We identified one Fe XIII line which has been assigned a wavelength in CHIANTI that is 0.7 Å longer than that given by Shirai et al. (2000) and entered in the NIST database. A line at this wavelength was observed in the spectrum returned by the SERTS 1995 flight (Brosius et al. 1998), and labeled as the Fe XIII line. However, this could be an Fe XII line instead, depending on which wavelength and identification one assumes. In fact, the wavelength of three Fe XII lines in the region we studied differ in CHIANTI and the NIST database. Resolving the actual wavelengths of these lines in the future should be of high priority; the good agreement we obtain with the CHIANTI model and wavelengths, however, favors the SERTS-95 identification over that given in the NIST database.

The density-sensitive line ratio $\lambda 203.8/\lambda 202.0$ has been shown to assume a value in the high-density limit that is close to that predicted by CHIANTI and our model with data by Aggarwal & Keenan. The ratio measured with EBIT is slightly larger than predicted by CHIANTI v5.2, while the observed line ratio from LHD is slightly smaller than predicted by CHIANTI v5.2. Since the density of LHD plasma is the order of 10^{13} cm^{-3} , the ratio should be at the high-density limit value. The lower value from LHD might be due to some other lines blended in at 202.0 and 203.8 Å, since we observed weak lines at these wavelengths when we observed without iron injection. If we take into account the contribution of these lines, the intensity ratio would be increased. Laboratory measurements at densities below 10^{11} cm^{-3} are needed to test the predictions of density-sensitive line ratios in a regime where most variation is expected.

This work was supported by the Solar and Heliospheric Physics Program of the National Aeronautics and Space Administration under grant NNX07AH986. Travel support was provided by National Science Foundation grant INT-0300708 and is gratefully acknowledged. Work at the Lawrence Livermore National Laboratory was performed under the auspices of the US Department of Energy under contract W-7405-Eng-48. This work was supported

by the research collaboration program in the National Institute for Fusion Science (NIFS05KYAM005). This work is supported by NIFS/NINS under the project of Formation of International Network for Scientific Collaborations. The collaboration program

at the National Institute for Fusion Science for LHD and *Solar-B/Hinode* is acknowledged. We are grateful to T. Watanabe at the National Astronomical Observatory of Japan of Japan for his encouragement and useful discussions.

REFERENCES

- Aggarwal, K. M., & Keenan, F. P. 2004, *A&A*, 418, 371
- Bar-Shalom, A., Klapisch, M., & Oreg, J. 2001, *J. Quant. Spectrosc. Radiat. Trans.*, 71, 179
- Beiersdorfer, P. 2003, *ARA&A* 412, 343
- Beiersdorfer, P., Crespo López-Urrutia, J. R., Springer, P., Utter, S. B., & Wong, K. L. 1999a, *Rev. Sci. Instrum.*, 70, 276
- Beiersdorfer, P., Lepson, J. K., Brown, G., Utter, S. B., Kahn, S., Liedahl, D., & Mauche, C. W. 1999b, *ApJ*, 519, L185
- Brickhouse, N. S., Raymond, J. C., & Smith, B. W. 1995, *ApJS*, 97, 551
- Brosius, J. W., Davila, J. M., & Thomas, R. J. 1998, *ApJS*, 119, 255
- Chen, H., Beiersdorfer, P., Heeter, L. A., Liedahl, D. A., Naranjo-Rivera, K. L., Träbert, E., Gu, M. F., & Lepson, J. K. 2004, *ApJ*, 611, 598
- Dere, K. P., Landi, E., Mason, H. E., Monsignori Fossi, B. C., & Young, P. R. 1997, *A&AS*, 125, 149
- Drake, J. J., Swartz, D. A., Beiersdorfer, P., Brown, G. V., & Kahn, S. M. 1999, *ApJ*, 521, 839
- Harada, T., & Kita, T. 1980, *Appl. Opt.*, 19, 3987
- Keenan, F. P., Jess, D. B., Aggarwal, K. M., Thomas, R. J., Brosius, J. W., & Davila, J. M. 2007, *MNRAS*, 376, 205
- Landi, E. 2002, *A&A*, 382, 1106
- Landi, E., Del Zanna, G., Young, P. R., Dere, K. P., Mason, H. E., & Landini, M. 2006, *ApJS*, 162, 261
- Landi, E., & Landini, M. 1997, *A&A*, 327, 1230
- Lepson, J. K., Beiersdorfer, P., Bitter, M., & Kahn, S. M. 2008, *Canadian J. Phys.*, 86, 175
- Lepson, J. K., Beiersdorfer, P., Brown, G. V., Liedahl, D. A., Brickhouse, N. S., Dupree, A. K., Kaastra, J. S., Mewe, R., & Kahn, S. M. 2002, *ApJ*, 578, 648
- Motojima, O., et al. 2005, *Nucl. Fusion*, 45 (Suppl.), 255
- Schmitt, J. H. M. M., Drake, J. J., Stern, R. A., & Haisch, B. M. 1996, *ApJ*, 457, 882
- Schwob, J. L., Wouters, A. W., Suckewer, S., & Finkenthal, M. 1987, *Rev. Sci. Instrum.*, 58, 1601
- Shirai, T., Sugar, J., Musgrove, A., & Wiese, W. L. 2000, *J. Phys. Chem. Ref. Data*, Monograph 8
- Skobelev, I., Murakami, I., & Kato, T. 2006, *NIFS-DATA*, 95, 1
- . 2007, *NIFS-DATA*, 99, 1
- Tamura, N., et al. 2003, *Plasma Phys. Control. Fusion*, 45, 27
- Thomas, R. J., & Neupert, W. M. 1994, *ApJS*, 91, 461
- Watanabe, T., Kato, T., Murakami, I., & Yamamoto, N. 2007, in *AIP Conf. Proc. 901, 5th International Conference on Atomic and Molecular Data and Their Applications (ICAMDATA)* (Melville: AIP), 215
- Young, B. K. F., Wilson, B. G., Price, D. F., & Stewart, R. E. 1998, *Phys. Rev. E*, 58, 4929
- Young, P. R. 2004, *A&A*, 417, 785
- Young, P. R., Mason, H. E., & Thomas, R. J. 1994, in *Solar Dynamic Phenomena and Solar Wind Consequences, the Third SOHO Workshop*, ed. J. J. Hunt (ESA SP-373; Garching: ESA), 417